Cell Reports
Physical Science

CellPress
OPEN ACCESS

Article

Nematic superconductivity from selective orbital pairing in iron pnictide single crystals

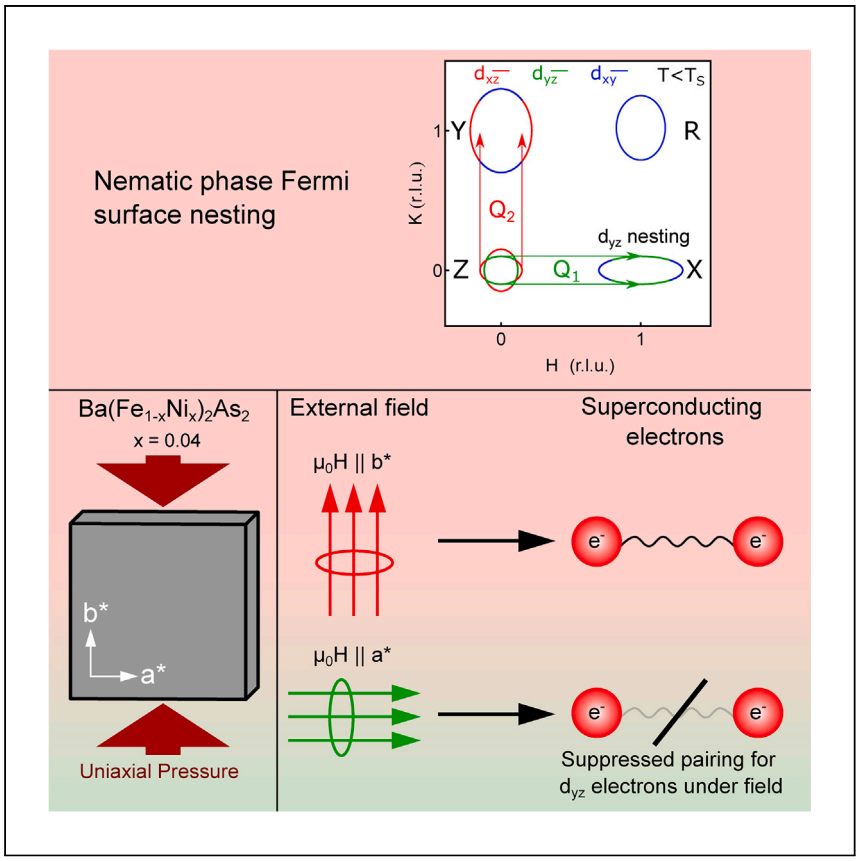

The discovery of iron-based superconductors proves that high-temperature superconductivity is not limited to cuprates. The findings here are consistent with an orbital pairing mechanism in iron-based superconductors, namely FeSe, contributing to a broader understanding of high-temperature superconductivity and its underlying mechanisms.

Mason L. Klemm, Shirin Mozaffari, Rui Zhang, ..., Ming Yi, Luis Balicas, Pengcheng Dai

balicas@magnet.fsu.edu (L.B.)
pdai@rice.edu (P.D.)

Highlights

Fermi surface nesting from prior work implies orbital-selective pairing

In-plane external field reveals anisotropy of T_c corresponding to nesting picture

Anisotropy of T_c disappears for samples in over-doped regime

Superconductivity in underdoped iron pnictides is orbital selective

Klemm et al., Cell Reports Physical Science 5, 101816
February 21, 2024
https://doi.org/10.1016/j.xcrp.2024.101816

Please cite this article in press as: Klemm et al., Nematic superconductivity from selective orbital pairing in iron pnictide single crystals, Cell Reports Physical Science (2024), https://doi.org/10.1016/j.xcrp.2024.101816

Cell Reports
Physical Science

Article

Nematic superconductivity from selective orbital pairing in iron pnictide single crystals

Mason L. Klemm,[1] Shirin Mozaffari,[2] Rui Zhang,[1] Brian W. Casas,[2] Alexei E. Koshelev,[3] Ming Yi,[1] Luis Balicas,[2,*] and Pengcheng Dai[1,4,*]

SUMMARY

The discovery of iron-based superconductors proves that high-temperature superconductivity is not limited to cuprates. Here, we use transport measurements to determine the in-plane anisotropy of the upper critical field (H_{c2}) in detwinned superconducting $Ba(Fe_{1-x}M_x)_2As_2$ (M = Co, Ni) single crystals. In previous measurements on twinned single crystals, the charge carrier doping dependence of the H_{c2} anisotropy for fields along inter-planar and in-plane directions was found to increase in the over-doped regime. For underdoped samples with a spin-nematic phase below the tetragonal-to-orthorhombic structural transition temperature, we find that H_{c2} along the *a* axis is considerably lower than that along the *b* axis. This H_{c2} anisotropy disappears in the over-doped regime when the system becomes tetragonal. By combining these results with previous works, we conclude that superconductivity in underdoped iron pnictides is orbital selective—with a dominant contribution from electrons with the d_{yz} orbital character and from being intimately associated with spin excitations.

INTRODUCTION

In conventional Bardeen-Cooper-Schrieffer (BCS) superconductors, electrons form coherent Cooper pairs below the superconducting transition temperature (T_c) through interacting with the lattice.[1] If the electrons forming Cooper pairs mostly originate from a single electronic band, the superconducting state is the ground state and does not coexist with charge- or spin-density wave order originating from the superconducting electronic band.[2] However, there are many multiband BCS superconductors, such as MgB_2,[3,4] and $NbSe_2$,[5,6] where superconductivity can occur in a specific band with an orbital-selective superconducting gap. While unconventional copper oxide superconductors are single-band materials,[7–9] iron-based superconductors are known multiband materials, where superconductivity may occur through an orbital-selective pairing mechanism analogous to that of multiband BCS superconductors.[10–13] Most unconventional superconductors, in contrast to BCS superconductors, have non-superconducting antiferromagnetic (AF) ordered parents, and superconductivity arises from electron/hole doping that suppresses the AF order.[7–9,14,15] In the case of iron pnictide superconductors, there is an additional tetragonal-to-orthorhombic structural phase transition at the structural transition temperature (T_s), occurring at or above the collinear static AF ordering temperature (T_N).[16] The structural transition is associated with an electronic nematic phase, where transport and electronic properties exhibit 2-fold rotational symmetry within the nearly square FeAs lattice[17–21] and orbital-dependent Fermi surface nesting.[22–28] With

[1]Department of Physics and Astronomy, Rice University, Houston, TX 77005, USA

[2]National High Magnetic Field Laboratory, Florida State University, Tallahassee, FL 32310, USA

[3]Materials Science Division, Argonne National Laboratory, Lemont, IL 60439, USA

[4]Lead contact

*Correspondence: balicas@magnet.fsu.edu (L.B.), pdai@rice.edu (P.D.)

https://doi.org/10.1016/j.xcrp.2024.101816

Please cite this article in press as: Klemm et al., Nematic superconductivity from selective orbital pairing in iron pnictide single crystals, Cell Reports Physical Science (2024), https://doi.org/10.1016/j.xcrp.2024.101816

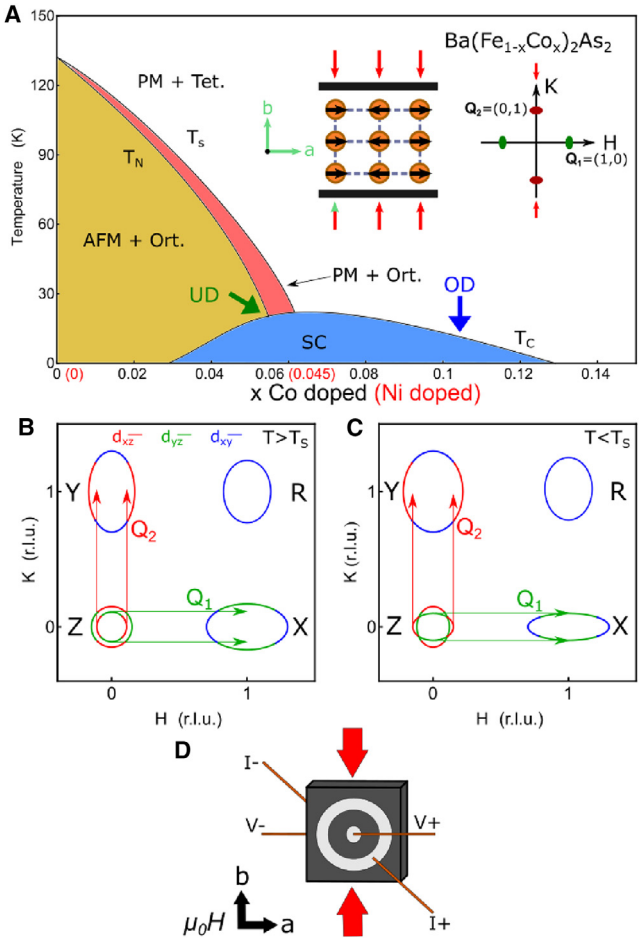

Figure 1. Phase diagram of electron-doped $BaFe_2As_2$ and associated Fermi surface evolution

(A) Phase diagram denoting the rough doping of the underdoped (UD) and over-doped (OD) samples. Note that the horizontal axis is modified for Ni-doped samples, as Ni contributes approximately twice as many electrons as Co. The first inset describes the orientation of the strain (red arrows) relative to the antiferromagnetic (AF) ordering defining the *a* and *b* axes. The second inset reflects the AF wavevector $\boldsymbol{Q_1}$ (green) and wavevector $\boldsymbol{Q_2}$ (red) studied in prior neutron scattering work.[29–32]

(B and C) Illustrative Fermi surfaces and associated orbital contributions for (B) the paramagnetic tetragonal lattice and the (C) nematic state below T_s for the simplified two-dimensional unfolded Brillouin zone. The arrows show the nesting wavevectors $\boldsymbol{Q_1}$ and $\boldsymbol{Q_2}$.

(D) Corbino geometry used to measure resistivity along the *c* axis. The back surface of the crystal is identically wired to that which is illustrated for the front surface.

increasing electron doping, T_s and T_N decrease and superconductivity appears, as shown schematically in Figure 1A for the $Ba(Fe_{1-x}M_x)_2As_2$ (M = Co, Ni) families of iron pnictide superconductors.[29–33] Given the close connection between magnetism and superconductivity, pairing in these superconducting materials is believed to be mediated by AF spin fluctuations,[14,15] arising from quasiparticle excitations between the sign-reversed hole and electron Fermi surfaces at different parts of the Brillouin zone.[34] This manifests experimentally as a resonance, or as collective magnetic excitation at an energy E_r appearing below the T_c with its intensity tracking the superconducting order parameter, in the spin-excitation spectra.[14,15,35–37] In the weak-coupling theory of superconductivity, the resonance is a bound state arising from quasiparticle excitations that connect parts of the Fermi surfaces exhibiting a sign

Please cite this article in press as: Klemm et al., Nematic superconductivity from selective orbital pairing in iron pnictide single crystals, Cell Reports Physical Science (2024), https://doi.org/10.1016/j.xcrp.2024.101816

change in the superconducting order parameter $\Delta(k) = -\Delta(k + Q)$, where $\Delta(k)$ is the momentum (k)-dependent superconducting gap and Q is the momentum transfer connecting the two gapped Fermi surfaces.[14,15,35–37]

The left inset in Figure 1A shows the collinear static AF structure of $BaFe_2As_2$, the parent compound of $Ba(Fe_{1-x}M_x)_2As_2$ families of iron pnictide superconductors.[15] In the underdoped regime, these materials exhibit a tetragonal-to-orthorhombic structural transition at T_s, a collinear static AF order below T_N, and superconductivity below T_c ($T_s > T_N > T_c$). When the doping reaches the optimal level for superconductivity (x = 0.06 [M = Co] and 0.04 [M = Ni]) and beyond, the system becomes tetragonal at all temperatures. With further doping increase, superconductivity vanishes for doping levels above x = 0.13 (M = Co) (Figure 1A).[29–33] For the iron pnictides, angle-resolved photoemission spectroscopy experiments reveal that three Fe t_{2g} orbitals (d_{xz}, d_{yz}, d_{xy}) are active near the Fermi level, forming hole and electron Fermi pockets as shown in Figure 1B.[13,38] Nesting among electron-hole Fermi surface sheets associated with quasiparticles on the d_{xz} and d_{yz} orbitals occurs along the Q_1 and Q_2 directions, respectively, and can induce spin excitations along these two directions.[39] In the paramagnetic tetragonal state, the degenerate d_{xz} and d_{yz} orbitals induce these spin excitations with equal intensity at Q_1 and Q_2. In the underdoped regime, upon cooling below T_s, the d_{yz} band of the electron Fermi surface at X/Y increases in energy, while the d_{xz} band decreases in energy.[40,41] Better nesting conditions resulting from the shifting of the bands lead to orbital-selective spin excitations for d_{yz} orbitals along the Q_1 direction.[42,43] Here, we note that while the AF order is also finite in the near-optimal underdoped region, angle-resolved photoemission spectroscopy measurements show the effect from the nematic order to be more prominent than that of the AF-ordered-induced folding.[24,44] Therefore, we only consider the dominant effect of the nematic order on the Fermi surfaces here. If the neutron spin resonance is associated with the superconducting electron pairing, then these results would suggest that superconductivity in iron arsenides and selenides is orbital selective[11,12,42,45,46] and dominated by the d_{yz} orbitals with associated AF fluctuations along the Q_1 direction. For underdoped $Ba(Fe_{1-x}M_x)_2As_2$, where superconductivity coexists microscopically with static AF order,[15] there is a reduction of static-ordered magnetic moment below T_c due to its competition with superconductivity.[29,47,48] Therefore, one would expect an anisotropic superconducting state within the orthorhombic lattice plane of the underdoped regime that disappears when the crystal becomes tetragonal in the over-doped regime without AF order at all temperatures. Here, using transport measurements, we report that the anisotropy of the in-plane upper critical fields (H_{c2}) of underdoped $Ba(Fe_{1-x}M_x)_2As_2$ is consistent with an orbital-selective pairing that involves electrons having d_{yz} orbital character.

RESULTS

Single-crystal preparation

The presence of twin domains in large single crystals of underdoped $Ba(Fe_{1-x}M_x)_2As_2$ renders conventional measurements insufficient to distinguish the rotational symmetry breaking between the d_{xz} and d_{yz} orbitals that occurs below T_s, meaning that neither orbital can be unambiguously determined to be associated with superconductivity in such a state. Therefore, uniaxial pressure must be used to obtain a single domain from which the intrinsic magnetic and electronic properties can be determined.[49] Electronic nematicity below T_s has long been established in the $Ba(Fe_{1-x}M_x)_2As_2$ materials through the process of detwinning.[17–21] The schematic provided in the left inset of Figure 1A details the in-plane AF ordering with respect

Please cite this article in press as: Klemm et al., Nematic superconductivity from selective orbital pairing in iron pnictide single crystals, Cell Reports Physical Science (2024), https://doi.org/10.1016/j.xcrp.2024.101816

to the direction of the applied uniaxial pressure. Recent neutron scattering experiments on detwinned, underdoped $Ba(Fe_{1-x}Co_x)_2As_2$ reveal anisotropic spin fluctuations, with the neutron spin resonance associated with superconductivity observed along the AF wavevector, $\boldsymbol{Q_1}$ = (1,0), and no magnetic scattering observed along $\boldsymbol{Q_2}$ = (0,1).[42] Additionally, the underdoped crystals experience a structural phase transition at T_s that changes the Fermi surface. It follows that the Fermi surface nesting is modified as a consequence of the transition (Figures 1B and 1C).[13,40] Although the H_{c2} anisotropy for in-plane and *c* axis-aligned magnetic fields has been heavily investigated for different families of iron-based superconductors,[33,50–57] there is no report of in-plane H_{c2} anisotropy for $Ba(Fe_{1-x}M_x)_2As_2$ having the orthorhombic lattice structure in the underdoped regime.

Single crystals were grown with $Fe_{1-x}M_xAs$ as the chosen flux via the self-flux method.[58] We chose to study underdoped $Ba(Fe_{1-x}Ni_x)_2As_2$ with x $\sim$ 0.04, which has a T_N ~44 K, where AF order coexists with superconductivity below T_c ~17 K,[48,59] and over-doped $Ba(Fe_{1-x}Co_x)_2As_2$ with x = 0.11.[30] Larger single crystals were aligned and later cut along the orthorhombic *a* and *b* axes into roughly 2 × 2 mm squares using a Laue X-ray diffractometer and a wire saw, respectively. Samples were then detwinned via uniaxial pressure with a small brass clamp. To investigate a potential orbital-selective pairing mechanism, we probe the anisotropy of the in-plane H_{c2}s of underdoped $Ba(Fe_{1-x}Ni_x)_2As_2$ via resistivity measurements along the *c* axis by using a Corbino geometry and an in-plane DC field (Figure 1D).[51] We use a Corbino-like geometry for the electrical contacts to maximize the cross-sectional area of the sample within the *ab* plane and to ensure a higher homogeneity for the electric current density flowing along the *c* axis. High current homogeneity and large cross-sectional areas are not achievable with other configurations for the electrical contacts. Field-dependent measurements of T_c were first conducted using the rotator option of a Quantum Design Physical Properties Measurement System, with the later measurements performed at the National High Magnetic Field Laboratory, using both a superconducting 18 T magnet and a 41 T resistive Bitter magnet, respectively. Our results reveal a clear anisotropy in the H_{c2}s of underdoped $Ba(Fe_{1-x}Ni_x)_2As_2$, with the field along the *a* axis resulting in a lower projected H_{c2} relative to fields aligned along the *b* axis (Figures 2, 3, and 4).

In-plane H_{c2} anisotropy measurements

To systematically characterize T_c, a range of magnetic fields were applied along the *a* and *b* axes of each sample, and then temperature was swept across the superconducting transition while maintaining a constant applied field. A schematic of the geometric relationship between the applied field direction, crystal axes, and strain direction is indicated in Figure 1D. It is clear from the raw resistivity data that a planar anisotropy exists in the underdoped samples (Figures 2A–2C and 2E). Traces of identical colors correspond to the same magnitude of the applied magnetic field with the lighter and darker shades of the same color representing the direction of the field, i.e., along the *a* and *b* axes, respectively. From these temperature sweeps, we extract the onset of T_c, which we define as 90% of the value of the resistivity in the normal state just above T_c. A sample-dependent, anomalous hump appears before the onset of superconductivity in some of our measurements. Strain-free measurements reveal that the hump only appears after pressure is applied to the sample (Figure S1). In these cases, we treat the 90% criterion as 90% of the normal state resistivity before the upturn of the humps (Figure 2A). Note that the apparent anisotropy depends on the definition of the onset, as reflected in a similar work.[54] Since the evaluation of the superconducting gap function would require an array of thermodynamic, spectroscopic, and transport techniques, transport measurements alone

Please cite this article in press as: Klemm et al., Nematic superconductivity from selective orbital pairing in iron pnictide single crystals, Cell Reports Physical Science (2024), https://doi.org/10.1016/j.xcrp.2024.101816

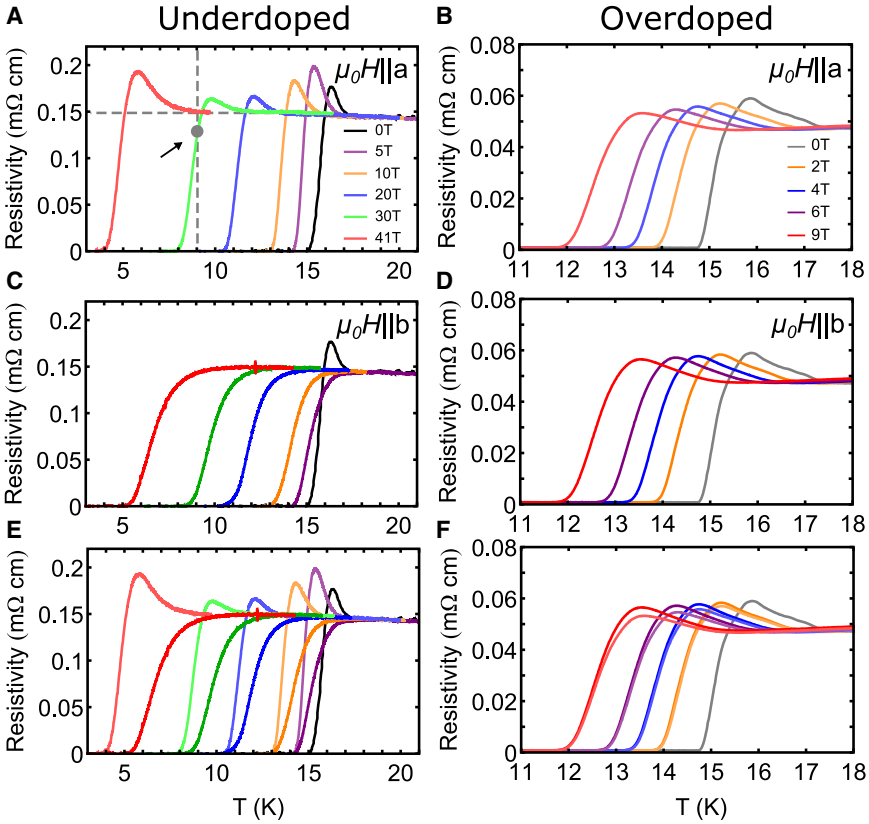

Figure 2. c axis transport measurements for different in-plane field directions

(A–F) Resistivity measured using a Corbino geometry (ρ_{zz}) as a function of the temperature under varying field strengths applied along the *a* axis for UD (A) and OD (B) samples. Data for field along the *b* axis for UD and OD samples are given in (C) and (D), respectively. (E) Same data as in (A) and (C) but plotted together to illustrate the anisotropy in upper critical fields (H_{c2}) inherent to the UD sample. Similarly, (B) and (D) are combined in (F) to illustrate the contrasting lack of anisotropy. Treatment of the 90% criterion in the presence of the humps is illustrated in (A), with the arrow noting the point on the curve at which the resistivity drops to 90% of its normal state value. Notice that the peaks preceding the superconducting transition are not observed in the absence of strain, with their presence along a specific field crystallographic orientation requiring further theoretical understanding. Notice also that at the highest magnetic fields, the zero-resistance state (vortex solid phase) is achieved at higher temperatures for both crystallographic orientations, implying that the observed anisotropy is unrelated to the flux flow of vortices. The normal state resistivity of the 41 T data in the UD sample was normalized to the normal state resistivity of the other curves.

cannot conclusively determine the absolute magnitude of the superconducting gap anisotropy. Nevertheless, from the transport measurements, we can evaluate the anisotropy of the characteristic energy scale required for thermally activated flux flow of vortices (Figure S5).

One important question to address is the impact of magnetic order and associated magnetoresistance to the observed H_{c2} anisotropy relative to fields aligned along the *a* and *b* axes. From in-plane magnetic field neutron diffraction measurements on twinned $Ba(Fe_{1-x}Ni_x)_2As_2$ with x ~0.04 (T_c = 17 K and $T_N \approx 44$ K), an identical doping level to our current transport measurements, an in-plane magnetic field of 10 T has no observable impact on magnetic-ordered moment, T_N, or spin fluctuations in the normal state (above T_c) but can recover superconductivity-suppressed static-magnetic-ordered moment below T_c.[48] Since the magnetoresistance in the

Please cite this article in press as: Klemm et al., Nematic superconductivity from selective orbital pairing in iron pnictide single crystals, Cell Reports Physical Science (2024), https://doi.org/10.1016/j.xcrp.2024.101816

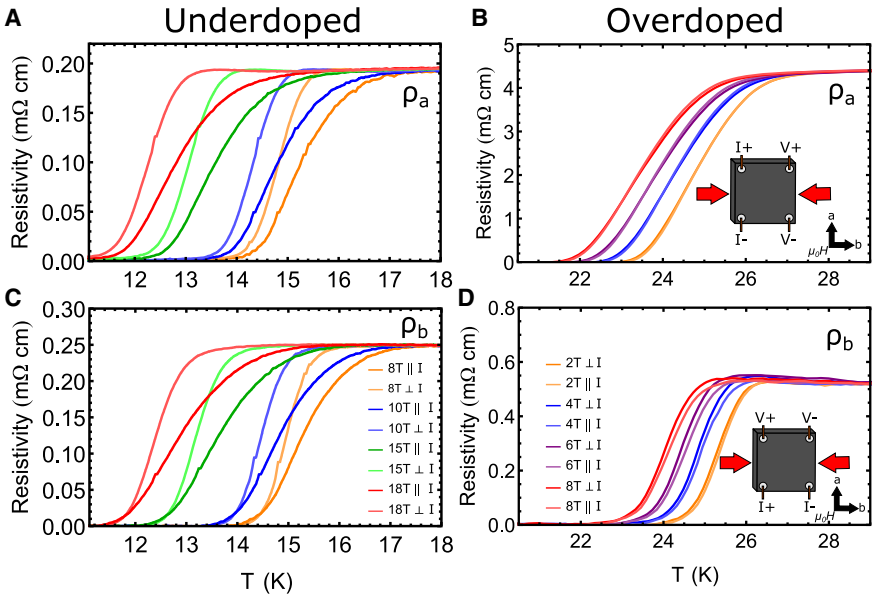

Figure 3. In-plane transport measurements for different in-plane field directions

(A–D) Resistive transitions as a function of T revealing the values of the H_{c2} ($\mu_0 H_{c2}$) for strain applied along the b axis. Data for theurrents along the a axis and for both planar field orientations for UD and OD samples are shown in (A) and (B), respectively. Data for the currents along the b axis are similarly presented for UD and OD samples in (C) and (D), respectively. Insets in (B) and (D) are schematics depicting the directions of the current (I+/−), strain (red arrows), and magnetic fields along crystalline axes a and b for each measurement. Regardless of the current orientation relative to strain, one always observes a larger inset field for currents aligned along the planar field.

normal (non-superconducting) state of $Ba(Fe_{1-x}Ni_x)_2As_2$ with x = 0.04 ($T \sim 18$ K) is at most 0.01% for a 20 T in-plane field and has no observable anisotropy for fields aligned along the a and b directions (Figures S6 and S7), we conclude that the observed H_{c2} anisotropy for fields aligned along the a and b axes in Figure 2 is due to the suppression of superconductivity and unrelated to the static AF order.

Because the electronic nematic phase is believed to be associated with the unidirectional spin resonance observed by inelastic neutron scattering, and thus the orbital-selective pairing, we can explore the over-doped side of the phase diagram to further test this hypothesis.[17,30,42,53] Over-doped single crystals experience no structural phase transitions associated with electronic nematicity but do retain a superconducting transition at a comparable T_c (Figure 1A). Identical resistivity measurements with uniaxial strain on over-doped samples reveal no anisotropy in the H_{c2}s like the one seen for the underdoped single crystals (Figures 2B–2D and 2F). Therefore, the anisotropy of H_{c2} observed in the underdoped sample and the lack thereof in the over-doped sample indicate that the observed anisotropic H_{c2} in the former is not due to applied uniaxial pressure but rather to the orbital-selective nature of the pairing contingent upon the existence of an electronic nematic phase.

The Montgomery method was utilized to capture the planar resistivity when the magnetic field is applied along either the a or b axis, as pictured in the inset of Figures 3B and 3D.[60,61] The purpose of these measurements is to test the differences in resistivity for current along and perpendicular to the applied magnetic field direction. Figures 3A and 3C summarize the results for underdoped single crystals with current along the a and b axes, respectively. While fields along the b axis suppress T_c more significantly than fields along the a axis according to inter-planar resistivity

Please cite this article in press as: Klemm et al., Nematic superconductivity from selective orbital pairing in iron pnictide single crystals, Cell Reports Physical Science (2024), https://doi.org/10.1016/j.xcrp.2024.101816

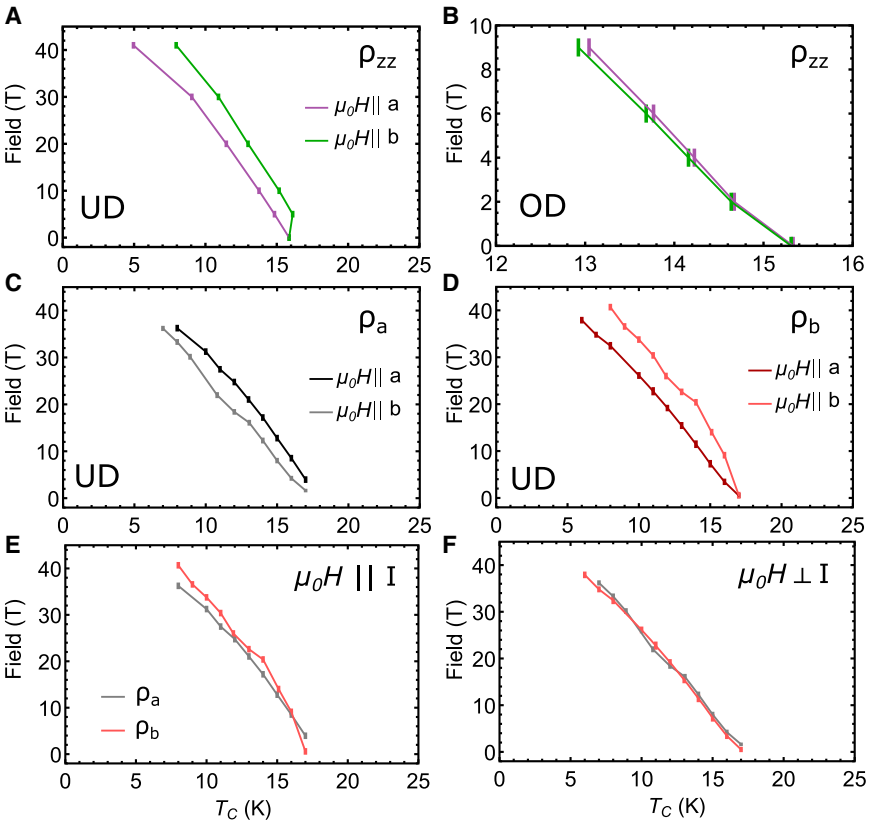

Figure 4. Temperature dependence of the H_{c2} anisotropy for UD and OD $BaFe_2As_2$

(A) H_{c2} as a function of the T when measured through the interplanar resistivity ρ_{zz} for an UD sample using the 90% criterion.

(B) $H_{c2}(T)$ for an OD sample as extracted from ρ_{zz}.

The insets for (A) and (B) display the extracted $H_{c2}(T)$ using the 50% criterion.

(C and D) H_{c2} for an UD sample as a function of T and as extracted from the in-plane resistivities, ρ_a and ρ_b, respectively.

(E and F) In-plane resistivity from (C) and (D) plotted such that the field and current are parallel and perpendicular, respectively. Error bars are assigned to the extracted H_{c2} to account for the humps. During the 90% criterion analysis, the normal state resistivity was considered from the peak of the hump to the flat region above the superconducting transition. The range of H_{c2} resulting from the different definitions of the normal state resistivity is what determines the size of the error bars. This is a liberal estimation of the measurement error. Notice that the anisotropy in H_{c2}s increases continuously as the temperature is lowered, in contrast to the anisotropy extracted for the activation energy for vortex flux flow (see Figure S5). Therefore, the anisotropy in H_{c2}s extracted using the 90% of the resistive transition criteria ought to be intrinsic or is unrelated to vortex physics.

measurements, the suppression of T_c as probed via the planar resistivity depends on the relative orientation between the field and the electrical currents. Specifically, T_c experiences a more dramatic suppression near the transition temperature when the applied field and the electric current are perpendicular to one another. A sample on the over-doped side with a slightly higher T_c, measured via this configuration, still reveals a very small anisotropy (Figures 3B–3D). The higher T_c of the over-doped samples is consistent with a closer proximity to the nematic phase, which vanishes near optimal superconductivity, compared to over-doped samples with the same T_c as that of the underdoped one (Figure 1A). In this configuration, one cannot exclude the possibility that this anisotropy might result from the relative alignment between the electrical currents and the external field or their interactions.

Please cite this article in press as: Klemm et al., Nematic superconductivity from selective orbital pairing in iron pnictide single crystals, Cell Reports Physical Science (2024), https://doi.org/10.1016/j.xcrp.2024.101816

Nevertheless, temperature sweeps for various applied currents reveal negligible differences in T_c, ruling out the magnitude of the current as being responsible for the observed anisotropy (Figure S2). Therefore, *c* axis resistivity is the most appropriate configuration to characterize this anisotropy because the relationship between the externally applied field and the electric current is maintained constant; in other words, they are always kept perpendicular to each other. In particular, there are clear differences in zero-resistance temperatures for fields applied along the *a* and *b* axes in the underdoped sample for fields above 20 T, when T_c is suppressed to below 10 K (Figure 2E). Since we do not have data above 20 T in the Montgomery method discussed in Figure 3, it is difficult to reach a conclusion about in-plane H_{c2} anisotropy using these results.

Further analysis on the raw data in Figure 2 was performed to extract the evolution of the onset T_c as a function of the increasing field for both underdoped and overdoped samples (Figures 4A and 4B). Clearly, the anisotropy in H_{c2} exists exclusively in the underdoped sample in this representation. The conditionality of the planar H_{c2} in the underdoped samples becomes more evident by plotting the T_c onset, demonstrating a faster suppression of the transport T_c near the zero-field transition temperature when the field and the electric current are perpendicular (Figure 4C and 4D). Plotting ρ_a and ρ_b when the field and current are parallel reveals minor anisotropy that increases at higher field (Figure 4E). The case where the field and electric current are perpendicular results in no anisotropy within error bars (Figure 4F).

DISCUSSION

In general, the anisotropy of the H_{c2} may be caused by either anisotropy of the Fermi velocity or the gap, and the first factor is more common. For the case of underdoped $Ba(Fe_{1-x}Ni_x)_2As_2$ materials with nematic order, several factors may contribute to the anisotropy of H_{c2}: (1) the hole bands become anisotropic, (2) anisotropies and occupations of the two electron bands become different, and (3) the interband pairings between the hole bands and two electron bands become different, leading to different superconducting gaps in the two electron bands. We believe that the last mechanism likely dominates due to strong modification of the nesting conditions upon entering the nematic state. Upon cooling from the normal state, the d_{yz} band along the Γ-X direction is lifted toward the Fermi energy (E_F), while the d_{xz} band along Γ-Y drops in energy relative to E_F, thus breaking the degeneracy between the two bands.[13] This should favor nesting between the Fermi surface sheets associated with the d_{yz} bands when compared to those of the d_{xz} bands, as illustrated in Figures 1B and 1C. Such a nesting condition would provide a clear explanation for the observed magnetic scattering along $\boldsymbol{Q_1}$ and $\boldsymbol{Q_2}$ in recent work.[42,43] If superconducting electron pairing in the iron pnictides is driven by spin fluctuations, as is widely suspected, we should expect pairing to occur as the result of d_{yz}-d_{yz} intra-orbital fluctuations, i.e., an orbital-selective pairing mechanism. A dramatic consequence of such a pairing mechanism would mean that the superconducting gaps are different for electrons with d_{yz} and d_{xz} orbital characters along the (1,0) and (0,1) directions, respectively. Therefore, we would also expect the H_{c2}s of this system, at which the superconducting pairing breaks down, to be directionally dependent between the (1,0) and (0,1) directions in the underdoped regime. Our results in Figure 4 reflect this anisotropy. It follows, then, that the over-doped single crystals should see no evidence of anisotropy among in-plane H_{c2}s, as these samples experience no transition into a nematic state and therefore no modification of the nesting condition in the band structure. Indeed, there is no H_{c2} anisotropy for over-doped samples under a similar uniaxial strain (Figure 4B). Therefore, our systematic H_{c2} measurements

Please cite this article in press as: Klemm et al., Nematic superconductivity from selective orbital pairing in iron pnictide single crystals, Cell Reports Physical Science (2024), https://doi.org/10.1016/j.xcrp.2024.101816

support the notion that superconductivity in the underdoped iron pnictide superconductors is orbital selective or clearly different from isotropic s-wave superconductors. These results are consistent with 2-fold oscillations of angular dependence of the in-plane and out-of-plane magnetoresistivity of $Ba_{0.5}K_{0.5}Fe_2As_2$ near T_c when the direction of the applied field is rotated within the plane.[62] We note that similar anisotropic H_{c2}s have been reported for twisted bilayer graphene as a sign of nematic superconducting pairing.[63] In that case, orbital-selective superconductivity is also the proposed mechanism, involving multicomponent pairing.[64]

We note that several Fe-based superconductors display H_{c2}s exceeding the Pauli limiting field.[50] The reason for this remains controversial, although it was often ascribed to the multiband nature of the superconductivity in these compounds. One possibility, particularly for more disordered chemically doped samples, is that this renormalization results from spin-orbit scattering, usually treated in terms of an isotropic spin-orbit scattering time (τ_{so}).[65] Alternatively, anisotropy of the potential scattering time may also contribute to the observed anisotropy.

It is well known that the scattering rate in the $Ba(Fe_{1-x}M_x)_2As_2$ family of Fe-based pnictide superconductors is rather anisotropic.[20,66,67] The reason for this anisotropy is not well understood, but it might reflect the intrinsic nematicity of the underlying electronic fluid from which superconductivity condenses.[68] In this scenario, one would expect that τ_{so} becomes anisotropic in the underdoped $Ba(Fe_{1-x}M_x)_2As_2$ compounds below T_N but above T_c, leading to the anisotropy in H_{c2}s observed here. However, we find a very small resistivity anisotropy associated with the electronic nematicity in the underdoped region of these compounds (see Figure S6).

In summary, we use a series of resistivity measurements to analyze the anisotropy of the in-plane H_{c2}s for uniaxial strain detwinned crystals of the iron pnictide superconductor $Ba(Fe_{1-x}M_x)_2As_2$. For underdoped samples with an orthorhombic lattice structure, we find a clear in-plane H_{c2} anisotropy in uniaxial strain detwinned samples for fields above 20 T with a c axis current. These results are consistent with an orbital-selective electron pairing, where the superconducting gap along the (1,0) direction with d_{yz} orbital character is larger than that along the (0,1) direction with d_{xz} orbital character. Therefore, superconductivity in the underdoped regime acquires a nematic character when it condenses from this electronic/spin state.[68] For the over-doped samples with a tetragonal lattice structure and without a nematic phase, similar measurements show no evidence of anisotropy in the in-plane H_{c2}s. These results are consistent with an orbital-selective pairing mechanism, suggesting that the quasiparticle excitations between electron-hole Fermi surface pockets having a d_{yz} orbital character are favorable for electron pairing. These results further confirm that superconductivity is likely mediated by spin fluctuations associated with the electron-hole quasiparticle excitations in iron-based superconductors.[14]

EXPERIMENTAL PROCEDURES

Resource availability

Lead contact

Further information and requests for resources should be directed to and will be fulfilled by the lead contact, Pengcheng Dai (pdai@rice.edu).

Materials availability

Compounds used in this study may be available from Pengcheng Dai (pdai@rice.edu) with a completed materials transfer agreement. Availability is subject to the current stocks in the laboratory.

Please cite this article in press as: Klemm et al., Nematic superconductivity from selective orbital pairing in iron pnictide single crystals, Cell Reports Physical Science (2024), https://doi.org/10.1016/j.xcrp.2024.101816

Data and code availability

All data reported in this paper will be shared by the lead authors upon request.

Sample synthesis

To prepare single crystals of $Ba(Fe_{1-x}M_x)_2As_2$, the flux and barium were mixed with a ratio of $Ba:Fe_{1-x}M_xAs = 1:4.5$ in an Al_2O_3 crucible and sealed under vacuum in a quartz tube. The tube was first warmed up to 900°C for 20 h, then to 1,175°C for 10 h, cooled to 1,050°C for 25 h, and lastly left to cool to room temperature with the furnace off. The underdoped samples were grown using Ni with x = 0.04, while the over-doped samples were grown using Co with x = 0.11. Larger crystals were aligned and later cut along the orthorhombic a and b axes into roughly 2 × 2 mm^2 using a Laue X-ray diffractometer and a wire saw, respectively.

Transport measurements

Figure S1 shows temperature dependence of the resistance for currents along a and b directions with in-plane fields with and without in-plane uniaxial pressure. Figure S2 shows current dependence of the resistance for underdoped sample with applied uniaxial pressure. Samples were then detwinned via uniaxial pressure with a small brass clamp (Figure S3).

Two additional over-doped samples were measured nearer to the optimal doping to demonstrate no/negligible anisotropy in the over-doped regime. Figure S4A shows an analogous plot to Figure 2 only with an over-doped sample with ~7% Co content. Figures S4B and S4C are analogous plots to Figure 3 but with nearly optimal doping of ~6.5%. Figure S5 shows resistivity across the superconducting transition. Figure S6 shows normal state field-dependent resistivity. Both Figures S5 and S6 are for $Ba(Fe_{1-x}Ni_x)_2As_2$ with the x ~0.04 sample. Figure S7 shows in-plane magnetic-field-dependent magnetoresistance in the normal state at 18 K, which is small and has no in-plane field directional dependence.

SUPPLEMENTAL INFORMATION

Supplemental information can be found online at https://doi.org/10.1016/j.xcrp.2024.101816.

ACKNOWLEDGMENTS

The experimental and basic materials synthesis work at Rice are supported by the US DOE, Basic Energy Sciences (BES), under grant no. DE-SC0012311 and by the Robert A. Welch Foundation under grant no. C-1839, respectively (P.D.). L.B. is supported by the US DOE, Basic Energy Sciences program through award DE-SC0002613. M.Y. acknowledges support by the Gordon and Betty Moore Foundation EPiQS Initiative through grant no. GBMF9470 and the Robert A. Welch Foundation, grant no. C-2175. The National High Magnetic Field Laboratory acknowledges support from the US-NSF cooperative agreement grant no. DMR-1644779 and the state of Florida. Work of A.E.K. at the Argonne National Laboratory was funded by the US DOE, Office of Science, BES, Materials Sciences and Engineering Division.

AUTHOR CONTRIBUTIONS

P.D. conceived the project. M.L.K. and R.Z. prepared the samples. High field experiments were carried out and analyzed by M.L.K., S.M., B.W.C., and L.B. Theoretical analysis was performed by A.E.K. The entire project was supervised by P.D., M.Y., and L.B. The manuscript was written by P.D., M.L.K., L.B., and A.E.K. All authors made comments.

DECLARATION OF INTERESTS

M.Y. is an advisory board member at *Cell Reports Physical Science*.

Received: September 8, 2023
Revised: October 30, 2023
Accepted: January 15, 2024
Published: February 6, 2024

REFERENCES

1. Bardeen, J., Cooper, L.N., and Schrieffer, J.R. (1957). Microscopic Theory of Superconductivity. Phys. Rev. *106*, 162–164. https://doi.org/10.1103/PhysRev.106.162.

2. Sipos, B., Kusmartseva, A.F., Akrap, A., Berger, H., Forró, L., and Tutiš, E. (2008). From Mott state to superconductivity in 1T-TaS_2. Nat. Mater. *7*, 960–965. https://doi.org/10.1038/nmat2318.

3. Nagamatsu, J., Nakagawa, N., Muranaka, T., Zenitani, Y., and Akimitsu, J. (2001). Superconductivity at 39 K in magnesium diboride. Nature *410*, 63–64. https://doi.org/10.1038/35065039.

4. Li, Q., Liu, B.T., Hu, Y.F., Chen, J., Gao, H., Shan, L., Wen, H.H., Pogrebnyakov, A.V., Redwing, J.M., and Xi, X.X. (2006). Large Anisotropic Normal-State Magnetoresistance in Clean MgB_2 Thin Films. Phys. Rev. Lett. *96*, 167003. https://doi.org/10.1103/PhysRevLett.96.167003.

5. Yokoya, T., Kiss, T., Chainani, A., Shin, S., Nohara, M., and Takagi, H. (2001). Fermi Surface Sheet-Dependent Superconductivity in 2H-$NbSe_2$. Science *294*, 2518–2520. https://doi.org/10.1126/science.1065068.

6. Heil, C., Poncé, S., Lambert, H., Schlipf, M., Margine, E.R., and Giustino, F. (2017). Origin of Superconductivity and Latent Charge Density Wave in NbS_2. Phys. Rev. Lett. *119*, 087003. https://doi.org/10.1103/PhysRevLett.119.087003.

7. Lee, P.A., Nagaosa, N., and Wen, X.-G. (2006). Doping a Mott insulator: Physics of high-temperature superconductivity. Rev. Mod. Phys. *78*, 17–85. https://doi.org/10.1103/RevModPhys.78.17.

8. Stewart, G.R. (2017). Unconventional superconductivity. Adv. Phys. *66*, 75–196. https://doi.org/10.1080/00018732.2017.1331615.

9. Keimer, B., Kivelson, S.A., Norman, M.R., Uchida, S., and Zaanen, J. (2015). From quantum matter to high-temperature superconductivity in copper oxides. Nature *518*, 179–186. https://doi.org/10.1038/nature14165.

10. Fernandes, R.M., Coldea, A.I., Ding, H., Fisher, I.R., Hirschfeld, P.J., and Kotliar, G. (2022). Iron pnictides and chalcogenides: a new paradigm for superconductivity. Nature *601*, 35–44. https://doi.org/10.1038/s41586-021-04073-2.

11. Sprau, P.O., Kostin, A., Kreisel, A., Böhmer, A.E., Taufour, V., Canfield, P.C., Mukherjee, S., Hirschfeld, P.J., Andersen, B.M., and Séamus Davis, J.C. (2017). Discovery of orbital-selective Cooper pairing in FeSe. Science *357*, 75–80. https://doi.org/10.1126/science.aal1575.

12. Nica, E.M., Yu, R., and Si, Q. (2017). Orbital-selective pairing and superconductivity in iron selenides. npj Quantum Mater. *2*, 24. https://doi.org/10.1038/s41535-017-0027-6.

13. Yi, M., Zhang, Y., Shen, Z.-X., and Lu, D. (2017). Role of the orbital degree of freedom in iron-based superconductors. npj Quantum Mater. *2*, 57. https://doi.org/10.1038/s41535-017-0059-y.

14. Scalapino, D.J. (2012). A common thread: The pairing interaction for unconventional superconductors. Rev. Mod. Phys. *84*, 1383–1417.

15. Dai, P. (2015). Antiferromagnetic order and spin dynamics in iron-based superconductors. Rev. Mod. Phys. *87*, 855–896. https://doi.org/10.1103/RevModPhys.87.855.

16. de la Cruz, C., Huang, Q., Lynn, J.W., Li, J., Ratcliff, W., II, Zarestky, J.L., Mook, H.A., Chen, G.F., Luo, J.L., Wang, N.L., and Dai, P. (2008). Magnetic order close to superconductivity in the iron-based layered $LaO_{1-x}F_xFeAs$ systems. Nature *453*, 899–902. https://doi.org/10.1038/nature07057.

17. Chu, J.-H., Analytis, J.G., de Greve, K., McMahon, P.L., Islam, Z., Yamamoto, Y., and Fisher, I.R. (2010). In-Plane Resistivity Anisotropy in an Underdoped Iron Arsenide Superconductor. Science *329*, 824–826. https://doi.org/10.1126/science.1190482.

18. Tanatar, M.A., Blomberg, E.C., Kreyssig, A., Kim, M.G., Ni, N., Thaler, A., Bud'ko, S.L., Canfield, P.C., Goldman, A.I., Mazin, I.I., and Prozorov, R. (2010). Uniaxial-strain mechanical detwinning of $CaFe_2As_2$ and $BaFe_2As_2$ crystals: Optical and transport study. Phys. Rev. B *81*, 184508.

19. Chuang, T.-M., Allan, M.P., Lee, J., Xie, Y., Ni, N., Bud'ko, S.L., Boebinger, G.S., Canfield, P.C., and Davis, J.C. (2010). Nematic Electronic Structure in the "Parent" State of the Iron-Based Superconductor $Ca(Fe_{1-x}Co_x)_2As_2$. Science *327*, 181–184. https://doi.org/10.1126/science.1181083.

20. Allan, M.P., Chuang, T.-M., Massee, F., Xie, Y., Ni, N., Bud'ko, S.L., Boebinger, G.S., Wang, Q., Dessau, D.S., Canfield, P.C., et al. (2013). Anisotropic impurity states, quasiparticle scattering and nematic transport in underdoped Ca(Fe1-xCox)2As2. Nat. Phys. *9*, 220–224. http://www.nature.com/nphys/journal/v9/n4/abs/nphys2544.html#supplementary-information.

21. Böhmer, A.E., Chu, J.-H., Lederer, S., and Yi, M. (2022). Nematicity and nematic fluctuations in iron-based superconductors. Nat. Phys. *18*, 1412–1419. https://doi.org/10.1038/s41567-022-01833-3.

22. Kim, Y., Oh, H., Kim, C., Song, D., Jung, W., Kim, B., Choi, H.J., Kim, C., Lee, B., Khim, S., et al. (2011). Electronic structure of detwinned $BaFe_2As_2$ from photoemission and first principles. Phys. Rev. B *83*, 064509. https://doi.org/10.1103/PhysRevB.83.064509.

23. Zhang, Y., He, C., Ye, Z.R., Jiang, J., Chen, F., Xu, M., Ge, Q.Q., Xie, B.P., Wei, J., Aeschlimann, M., et al. (2012). Symmetry breaking via orbital-dependent reconstruction of electronic structure in detwinned NaFeAs. Phys. Rev. B *85*, 085121.

24. Ge, Q.Q., Ye, Z.R., Xu, M., Zhang, Y., Jiang, J., Xie, B.P., Song, Y., Zhang, C.L., Dai, P., Feng, D.L., et al. (2013). Anisotropic but Nodeless Superconducting Gap in the Presence of Spin-Density Wave in Iron-Pnictide Superconductor $NaFe_{1-x}Co_xAs$. Phys. Rev. X *3*, 011020. https://doi.org/10.1103/PhysRevX.3.011020.

25. Suzuki, Y., Shimojima, T., Sonobe, T., Nakamura, A., Sakano, M., Tsuji, H., Omachi, J., Yoshioka, K., Kuwata-Gonokami, M., Watashige, T., et al. (2015). Momentum-dependent sign inversion of orbital order in superconducting FeSe. Phys. Rev. B *92*, 205117. https://doi.org/10.1103/PhysRevB.92.205117.

26. Pfau, H., Chen, S.D., Yi, M., Hashimoto, M., Rotundu, C.R., Palmstrom, J.C., Chen, T., Dai, P.-C., Straquadine, J., Hristov, A., et al. (2019). Momentum Dependence of the Nematic Order Parameter in Iron-Based Superconductors. Phys. Rev. Lett. *123*, 066402. https://doi.org/10.1103/PhysRevLett.123.066402.

27. Watson, M.D., Kim, T.K., Rhodes, L.C., Eschrig, M., Hoesch, M., Haghighirad, A.A., and Coldea, A.I. (2016). Evidence for unidirectional nematic bond ordering in FeSe. Phys. Rev. B *94*, 201107. https://doi.org/10.1103/PhysRevB.94.201107.

28. Yi, M., Pfau, H., Zhang, Y., He, Y., Wu, H., Chen, T., Ye, Z., Hashimoto, M., Yu, R., Si, Q., et al. (2019). Nematic Energy Scale and the Missing Electron Pocket in FeSe. Phys. Rev. X *9*, 041049. https://doi.org/10.1103/PhysRevX.9.041049.

29. Pratt, D.K., Tian, W., Kreyssig, A., Zarestky, J.L., Nandi, S., Ni, N., Bud'ko, S.L., Canfield, P.C., Goldman, A.I., and McQueeney, R.J. (2009). Coexistence of Competing Antiferromagnetic and Superconducting Phases in the Underdoped $Ba(Fe_{0.953}Co_{0.047})_2As_2$

Compound Using X-ray and Neutron Scattering Techniques. Phys. Rev. Lett. *103*, 087001. https://doi.org/10.1103/PhysRevLett.103.087001.

30. Nandi, S., Kim, M.G., Kreyssig, A., Fernandes, R.M., Pratt, D.K., Thaler, A., Ni, N., Bud'ko, S.L., Canfield, P.,C., Schmalian, J., et al. (2010). Anomalous Suppression of the Orthorhombic Lattice Distortion in Superconducting $Ba(Fe_{1-x}Co_x)_2As_2$ Single Crystals. Phys. Rev. Lett. *104*, 057006. https://doi.org/10.1103/PhysRevLett.104.057006.

31. Luo, H., Yamani, Z., Chen, Y., Lu, X., Wang, M., Li, S., Maier, T.A., Danilkin, S., Adroja, D.T., and Dai, P. (2012). Electron doping evolution of the anisotropic spin excitations in $BaFe_{2-x}Ni_xAs_2$. Phys. Rev. B *86*, 024508. https://doi.org/10.1103/PhysRevB.86.024508.

32. Lu, X., Gretarsson, H., Zhang, R., Liu, X., Luo, H., Tian, W., Laver, M., Yamani, Z., Kim, Y.-J., Nevidomskyy, A.H., et al. (2013). Avoided Quantum Criticality and Magnetoelastic Coupling in $BaFe_{2-x}Ni_xAs_2$. Phys. Rev. Lett. *110*, 257001. https://doi.org/10.1103/PhysRevLett.110.257001.

33. Ni, N., Thaler, A., Yan, J.Q., Kracher, A., Colombier, E., Bud'ko, S.L., Canfield, P.C., and Hannahs, S.T. (2010). Temperature versus doping phase diagrams for $Ba(Fe_{1-x}TM_x)_2As_2$ (TM=Ni,Cu, Cu/Co) single crystals. Phys. Rev. B *82*, 024519. https://doi.org/10.1103/PhysRevB.82.024519.

34. Hirschfeld, P.J., Korshunov, M.M., and Mazin, I.I. (2011). Gap symmetry and structure of Fe-based superconductors. Rep. Prog. Phys. *74*, 124508.

35. Eschrig, M. (2006). The effect of collective spin-1 excitations on electronic spectra in high T_c superconductors. Adv. Phys. *55*, 47–183.

36. Yu, G., Li, Y., Motoyama, E.M., and Greven, M. (2009). A universal relationship between magnetic resonance and superconducting gap in unconventional superconductors. Nat. Phys. *5*, 873–875. http://www.nature.com/nphys/journal/v5/n12/suppinfo/nphys1426_S1.html.

37. Duan, C., Baumbach, R.E., Podlesnyak, A., Deng, Y., Moir, C., Breindel, A.J., Maple, M.B., Nica, E.M., Si, Q., and Dai, P. (2021). Resonance from antiferromagnetic spin fluctuations for superconductivity in UTe_2. Nature *600*, 636–640. https://doi.org/10.1038/s41586-021-04151-5.

38. Yi, M., Lu, D., Chu, J.-H., Analytis, J.G., Sorini, A.P., Kemper, A.F., Moriz, B., Mo, S.-K., Moore, R.G., Hashimoto, M., et al. (2011). Symmetry-breaking orbital anisotropy observed for detwinned $Ba(Fe_{1-x}Co_x)_2As_2$ above the spin density wave transition. Proc. Natl. Acad. Sci. USA *108*, 6878–6883. https://doi.org/10.1073/pnas.1015572108.

39. Dai, P., Hu, J., and Dagotto, E. (2012). Magnetism and its microscopic origin in iron-based high-temperature superconductors. Nat. Phys. *8*, 709–718. https://doi.org/10.1038/nphys2438.

40. Pfau, H., Rotundu, C.R., Palmstrom, J.C., Chen, S.D., Hashimoto, M., Lu, D., Kemper, A.F., Fisher, I.R., and Shen, Z., -X. (2019). Detailed band structure of twinned and detwinned $BaFe_2As_2$ studied with angle-resolved photoemission spectroscopy. Phys. Rev. B *99*, 035118. https://doi.org/10.1103/PhysRevB.99.035118.

41. Watson, M.D., Dudin, P., Rhodes, L.C., Evtushinsky, D.V., Iwasawa, H., Aswartham, S., Wurmehl, S., Büchner, B., Hoesch, M., and Kim, T.K. (2019). Probing the reconstructed Fermi surface of antiferromagnetic $BaFe_2As_2$ in one domain. npj Quantum Mater. *4*, 36. https://doi.org/10.1038/s41535-019-0174-z.

42. Tian, L., Liu, P., Xu, Z., Li, Y., Lu, Z., Walker, H.C., Stuhr, U., Tan, G., Lu, X., and Dai, P. (2019). Spin fluctuation anisotropy as a probe of orbital-selective hole-electron quasiparticle excitations in detwinned $Ba(Fe_{1-x}Co_x)_2As_2$. Phys. Rev. B *100*, 134509. https://doi.org/10.1103/PhysRevB.100.134509.

43. Tam, D.W., Yin, Z., Xie, Y., Wang, W., Stone, M.B., Adroja, D.T., Walker, H.C., Yi, M., and Dai, P. (2020). Orbital selective spin waves in detwinned NaFeAs. Phys. Rev. B *102*, 054430. https://doi.org/10.1103/PhysRevB.102.054430.

44. Liu, C., Kondo, T., Fernandes, R.M., Palczewski, A.D., Mun, E.D., Ni, N., Thaler, A.N., Bostwick, A., Rotenberg, E., Schmalian, J., et al. (2010). Evidence for a Lifshitz transition in electron-doped iron arsenic superconductors at the onset of superconductivity. Nat. Phys. *6*, 419–423. http://www.nature.com/nphys/journal/v6/n6/abs/nphys1656.html#supplementary-information.

45. Chen, T., Chen, Y., Kreisel, A., Lu, X., Schneidewind, A., Qiu, Y., Park, J.T., Perring, T.G., Stewart, J.R., Cao, H., et al. (2019). Anisotropic spin fluctuations in detwinned FeSe. Nat. Mater. *18*, 709–716. https://doi.org/10.1038/s41563-019-0369-5.

46. Kreisel, A., Mukherjee, S., Hirschfeld, P.J., and Andersen, B.M. (2015). Spin excitations in a model of FeSe with orbital ordering. Phys. Rev. B *92*, 224515. https://doi.org/10.1103/PhysRevB.92.224515.

47. Christianson, A.D., Lumsden, M.D., Nagler, S.E., MacDougall, G.J., McGuire, M.A., Sefat, A.S., Jin, R., Sales, B.C., and Mandrus, D. (2009). Static and Dynamic Magnetism in Underdoped Superconductor $BaFe_{1.92}Co_{0.08}As_2$. Phys. Rev. Lett. *103*, 087002.

48. Wang, M., Luo, H., Wang, M., Chi, S., Rodriguez-Rivera, J.A., Singh, D., Chang, S., Lynn, J.W., and Dai, P. (2011). Magnetic field effect on static antiferromagnetic order and spin excitations in the underdoped iron arsenide superconductor $BaFe_{1.92}Ni_{0.08}As_2$. Phys. Rev. B *83*, 094516. https://doi.org/10.1103/PhysRevB.83.094516.

49. Fisher, I.R., Degiorgi, L., and Shen, Z.X. (2011). In-plane electronic anisotropy of underdoped '122' Fe-arsenide superconductors revealed by measurements of detwinned single crystals. Rep. Prog. Phys. *74*, 124506.

50. Yuan, H.Q., Singleton, J., Balakirev, F.F., Baily, S.A., Chen, G.F., Luo, J.L., and Wang, N.L. (2009). Nearly isotropic superconductivity in $(Ba,K)Fe_2As_2$. Nature *457*, 565–568. https://doi.org/10.1038/nature07676.

51. Wang, X.F., Wu, T., Wu, G., Chen, H., Xie, Y.L., Ying, J.J., Yan, Y.J., Liu, R.H., and Chen, X.H. (2009). Anisotropy in the Electrical Resistivity and Susceptibility of Superconducting $BaFe_2As_2$ Single Crystals. Phys. Rev. Lett. *102*, 117005. https://doi.org/10.1103/PhysRevLett.102.117005.

52. Her, J.L., Kohama, Y., Matsuda, Y.H., Kindo, K., Yang, W.-H., Chareev, D.A., Mitrofanova, E.S., Volkova, O.S., Vasiliev, A.N., and Lin, J.-Y. (2015). Anisotropy in the upper critical field of FeSe and $FeSe_{0.33}Te_{0.67}$single crystals. Supercond. Sci. Technol. *28*, 045013. https://doi.org/10.1088/0953-2048/28/4/045013.

53. Wang, Z., Xie, T., Kampert, E., Förster, T., Lu, X., Zhang, R., Gong, D., Li, S., Herrmannsdörfer, T., Wosnitza, J., and Luo, H. (2015). Electron doping dependence of the anisotropic superconductivity in $BaFe_{2-x}Ni_xAs_2$. Phys. Rev. B *92*, 174509. https://doi.org/10.1103/PhysRevB.92.174509.

54. Llovo, I.F., Carballeira, C., Sóñora, D., Pereiro, A., Ponte, J.J., Salem-Sugui, S., Jr., Sefat, A.S., and Mosqueira, J. (2021). Multiband effects on the upper critical field angular dependence of 122-family iron pnictide superconductors. Sci. Rep. *11*, 11526. https://doi.org/10.1038/s41598-021-90858-4.

55. Welp, U., Xie, R., Koshelev, A.E., Kwok, W.K., Luo, H.Q., Wang, Z.S., Mu, G., and Wen, H.H. (2009). Anisotropic phase diagram and strong coupling effects in $Ba_{1-x}K_xFe_2As_2$ from specific-heat measurements. Phys. Rev. B *79*, 094505. https://doi.org/10.1103/PhysRevB.79.094505.

56. Murphy, J., Tanatar, M.A., Graf, D., Brooks, J.S., Bud'ko, S.L., Canfield, P.C., Kogan, V.G., and Prozorov, R. (2013). Angular-dependent upper critical field of overdoped $Ba(Fe_{1-x}Ni_x)_2As_2$. Phys. Rev. B *87*, 094505. https://doi.org/10.1103/PhysRevB.87.094505.

57. Gurevich, A. (2011). Iron-based superconductors at high magnetic fields. Rep. Prog. Phys. *74*, 124501. https://doi.org/10.1088/0034-4885/74/12/124501.

58. Luo, H., Lu, X., Zhang, R., Wang, M., Goremychkin, E.A., Adroja, D.T., Danilkin, S., Deng, G., Yamani, Z., and Dai, P. (2013). Electron doping evolution of the magnetic excitations in $BaFe_{2-x}Ni_xAs_2$. Phys. Rev. B *88*, 144516. https://doi.org/10.1103/PhysRevB.88.144516.

59. Luo, H., Zhang, R., Laver, M., Yamani, Z., Wang, M., Lu, X., Wang, M., Chen, Y., Li, S., Chang, S., et al. (2012). Coexistence and Competition of the Short-Range Incommensurate Antiferromagnetic Order with the Superconducting State of $BaFe_{2-x}Ni_xAs_2$. Phys. Rev. Lett. *108*, 247002. https://doi.org/10.1103/PhysRevLett.108.247002.

60. Montgomery, H.C. (1971). Method for Measuring Electrical Resistivity of Anisotropic Materials. J. Appl. Phys. *42*, 2971–2975. https://doi.org/10.1063/1.1660656.

61. dos Santos, C.A.M., de Campos, A., da Luz, M.S., White, B.D., Neumeier, J.J., de Lima, B.S., and Shigue, C.Y. (2011). Procedure for measuring electrical resistivity of anisotropic materials: A revision of the Montgomery method. J. Appl. Phys. *110*, 083703. https://doi.org/10.1063/1.3652905.

62. Li, J., Pereira, P.J., Yuan, J., Lv, Y.-Y., Jiang, M.-P., Lu, D., Lin, Z.-Q., Liu, Y.-J., Wang, J.-F.,

Li, L., et al. (2017). Nematic superconducting state in iron pnictide superconductors. Nat. Commun. *8*, 1880. https://doi.org/10.1038/s41467-017-02016-y.

63. Cao, Y., Rodan-Legrain, D., Park, J.M., Yuan, N.F.Q., Watanabe, K., Taniguchi, T., Fernandes, R.M., Fu, L., and Jarillo-Herrero, P. (2021). Nematicity and competing orders in superconducting magic-angle graphene. Science *372*, 264–271. https://doi.org/10.1126/science.abc2836.

64. Lake, E., Patri, A.S., and Senthil, T. (2022). Pairing symmetry of twisted bilayer graphene: A phenomenological synthesis. Phys. Rev. B *106*, 104506. https://doi.org/10.1103/PhysRevB.106.104506.

65. Tinkham, M. (2004). Introduction to Superconductivity (Dover Publications).

66. Ishida, S., Nakajima, M., Liang, T., Kihou, K., Lee, C.H., Iyo, A., Eisaki, H., Kakeshita, T., Tomioka, Y., Ito, T., and Uchida, S. (2013). Anisotropy of the In-Plane Resistivity of Underdoped $Ba(Fe_{1-x}Co_x)_2As_2$ Superconductors Induced by Impurity Scattering in the Antiferromagnetic Orthorhombic Phase. Phys. Rev. Lett. *110*, 207001. https://doi.org/10.1103/PhysRevLett.110.207001.

67. Rosenthal, E.P., Andrade, E.F., Arguello, C.J., Fernandes, R.M., Xing, L.Y., Wang, X.C., Jin, C.Q., Millis, A.J., and Pasupathy, A.N. (2014). Visualization of electron nematicity and unidirectional antiferroic fluctuations at high temperatures in NaFeAs. Nat. Phys. *10*, 225–232. https://doi.org/10.1038/nphys2870.

68. Schmidt, J., Bekeris, V., Lozano, G.S., Bortulé, M.V., Bermúdez, M.M., Hicks, C.W., Canfield, P.C., Fradkin, E., and Pasquini, G. (2019). Nematicity in the superconducting mixed state of strain detwinned underdoped $Ba(Fe_{1-x}Co_x)_2As_2$. Phys. Rev. B *99*, 064515. https://doi.org/10.1103/PhysRevB.99.064515.

Cell Reports Physical Science, Volume *5*

Supplemental information

Nematic superconductivity from selective orbital pairing in iron pnictide single crystals

Mason L. Klemm, Shirin Mozaffari, Rui Zhang, Brian W. Casas, Alexei E. Koshelev, Ming Yi, Luis Balicas, and Pengcheng Dai

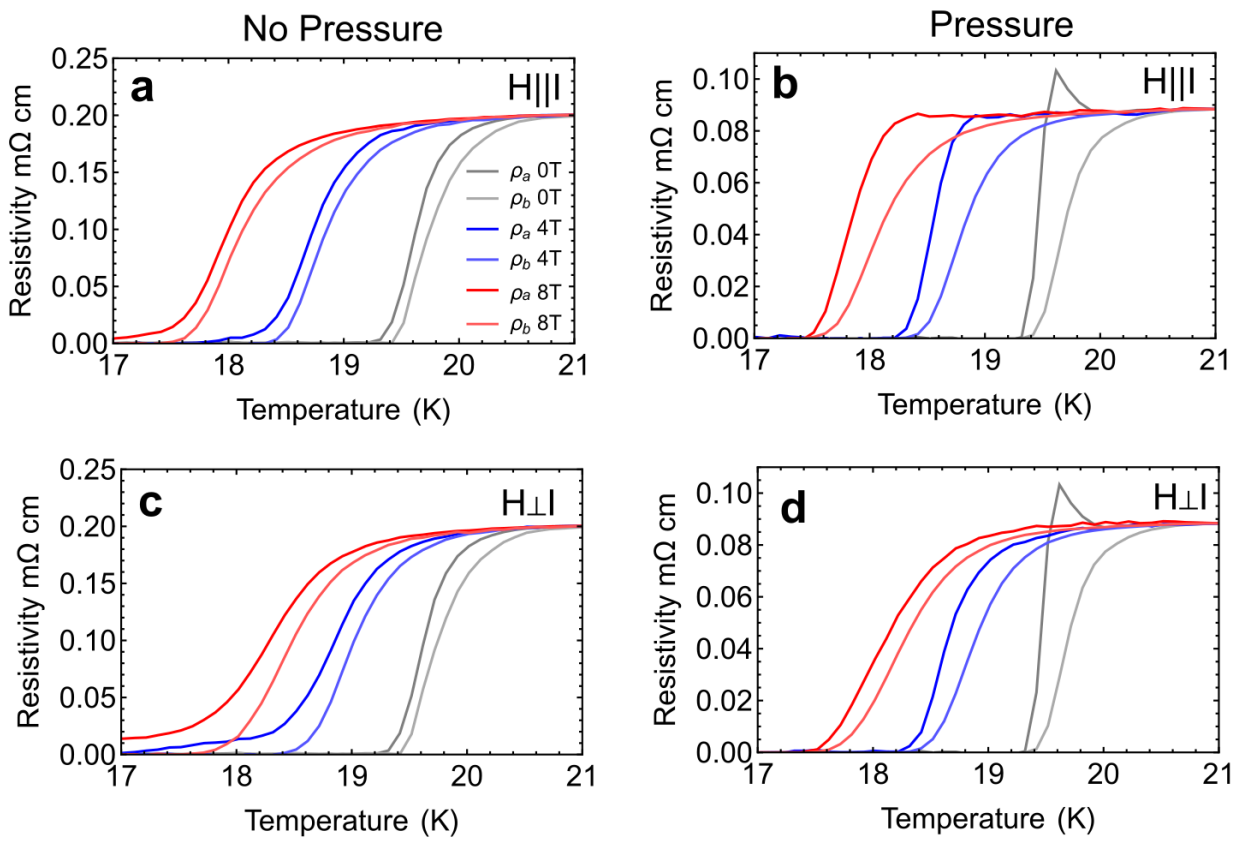

Fig. S1: **Comparison of transport measurements with and without uniaxial pressure (strain).** (a) In-plane resistivity anisotropy with the field aligned along the current direction in the absence of strain. (b) With strain applied, the in-plane resistivity anisotropy with the field aligned along the current direction. (c) and (d) are the analogs to (a) and (b), respectively, with the field now aligned perpendicularly to the current.

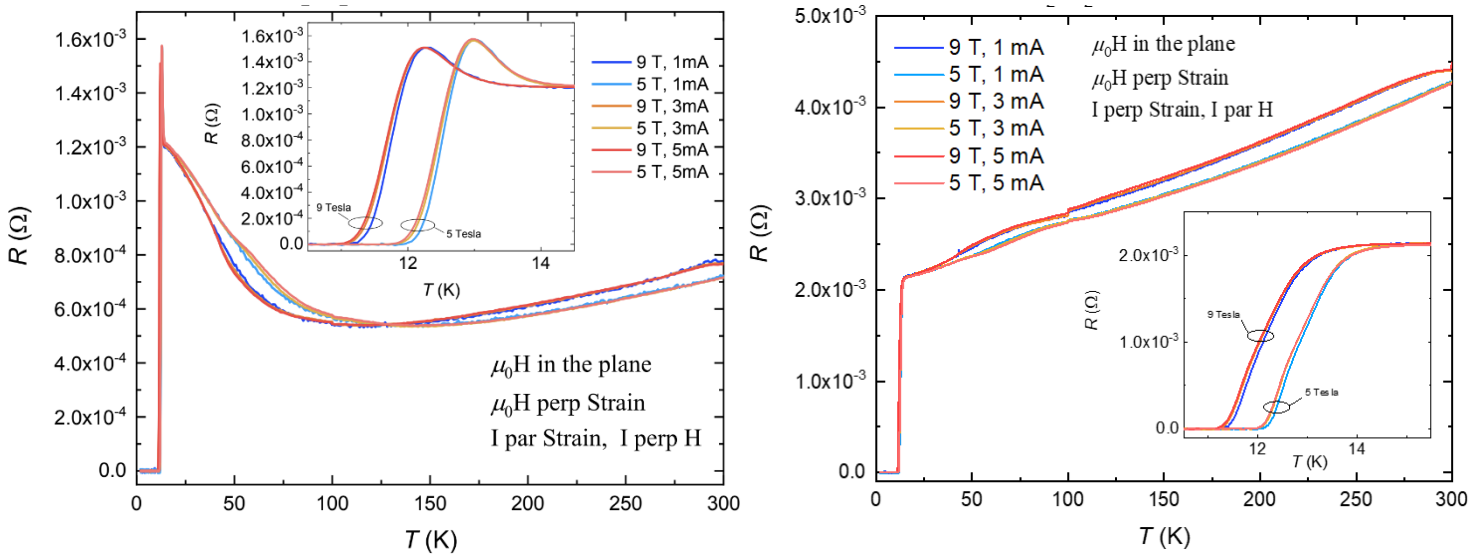

Fig. S2: **Current dependence of an underdoped sample using Montgomery method**. Current dependence of the resistance of an underdoped sample showing resistivity along b (left) and a (right) axes. Three different currents (1, 3, & 5 mA) were measured at two fields (5,9 T). Inset highlights the temperature region immediately surrounding T_c.

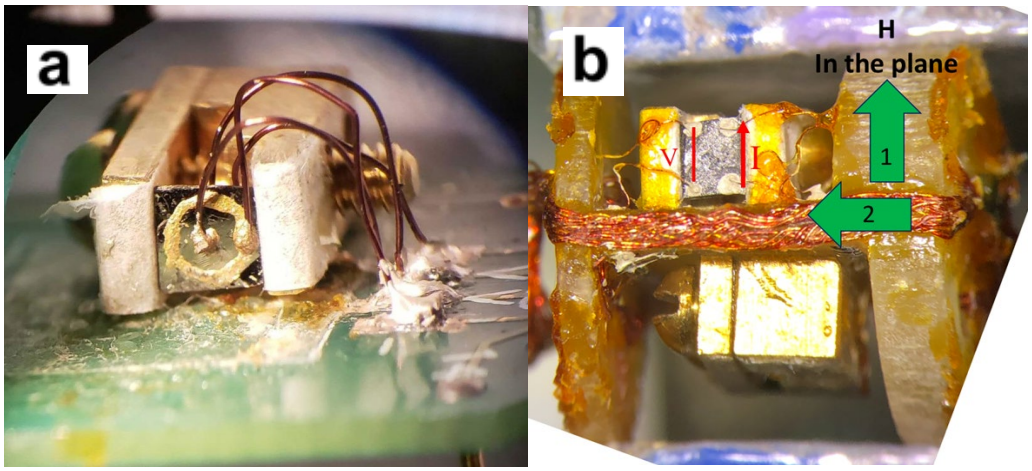

Fig. S3: **Example of sample wiring configurations.** Single crystal mounted on a brass clamp and wired in a Corbino geometry mounted on a Physical Property Measurements System puck (a). Two single crystals in two brass clamps mounted for measurements at the MagLab, with a diagram depicting voltage and current configuration for ρ_a (b).

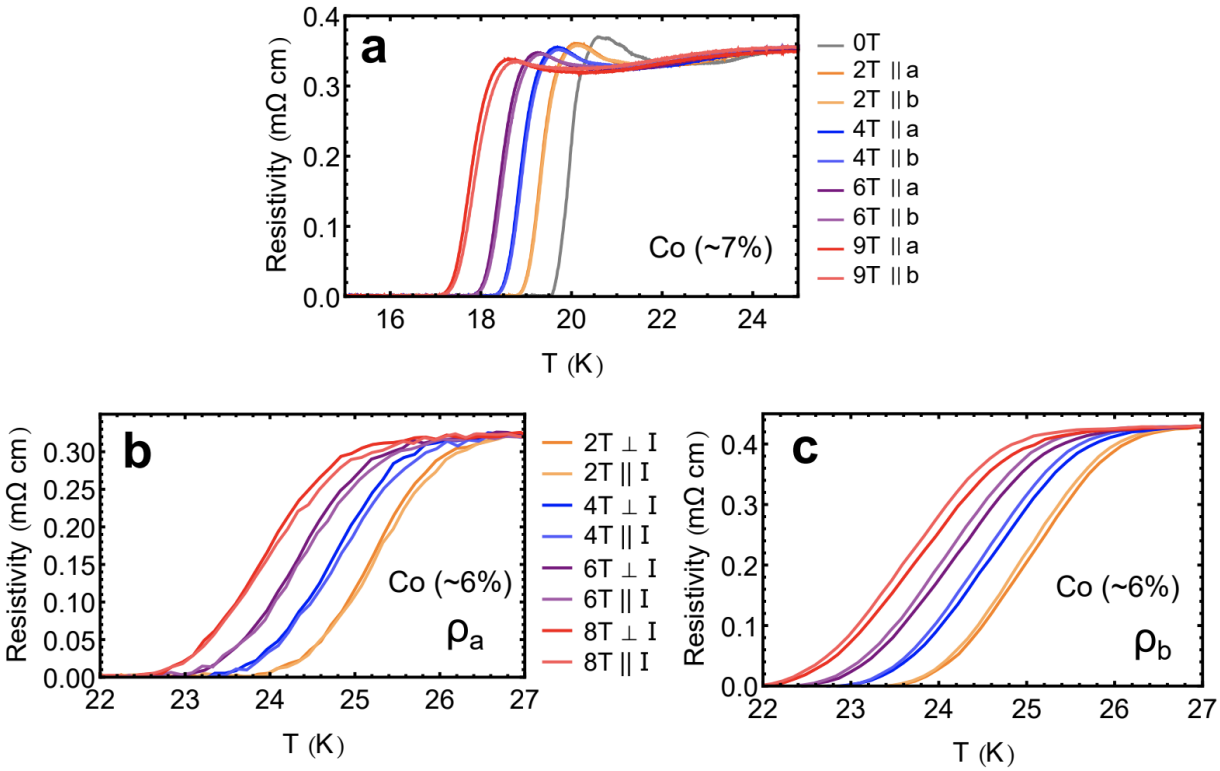

Fig. S4: **Overdoped resistivity anisotropy for samples doped close to the nematic phase boundary.** (a) Overdoped sample measured with current along the *c*-axis using a Corbino geometry with roughly 7% Co-doping. (b,c) Resistivity ρ_a and ρ_b, respectively, as a function of temperature for distinct orientations of the current relative to field for a different overdoped sample, close to optimally doped ~6% Co.

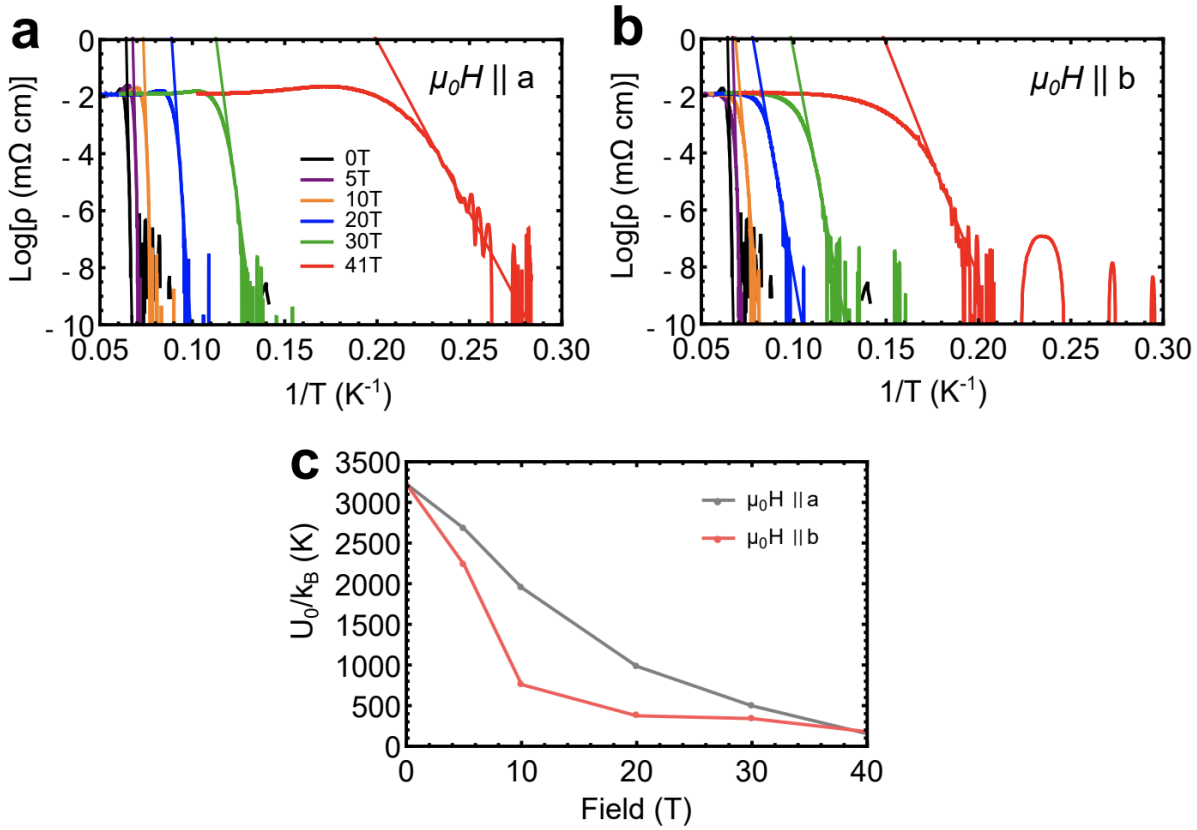

Fig. S5: **Activation energy extraction for underdoped high-field data.** (a) Resistivity across the superconducting transition in a logarithmic scale and for fields along the *a*-axis, as a function of the inverse temperature. Straight lines are linear fits from which we extract the activation energy U_0 for vortex flow. (b) Same as in (a) but for fields along the *b*-axis. (c) U_0/k_B as a function of magnetic field for both field orientations.

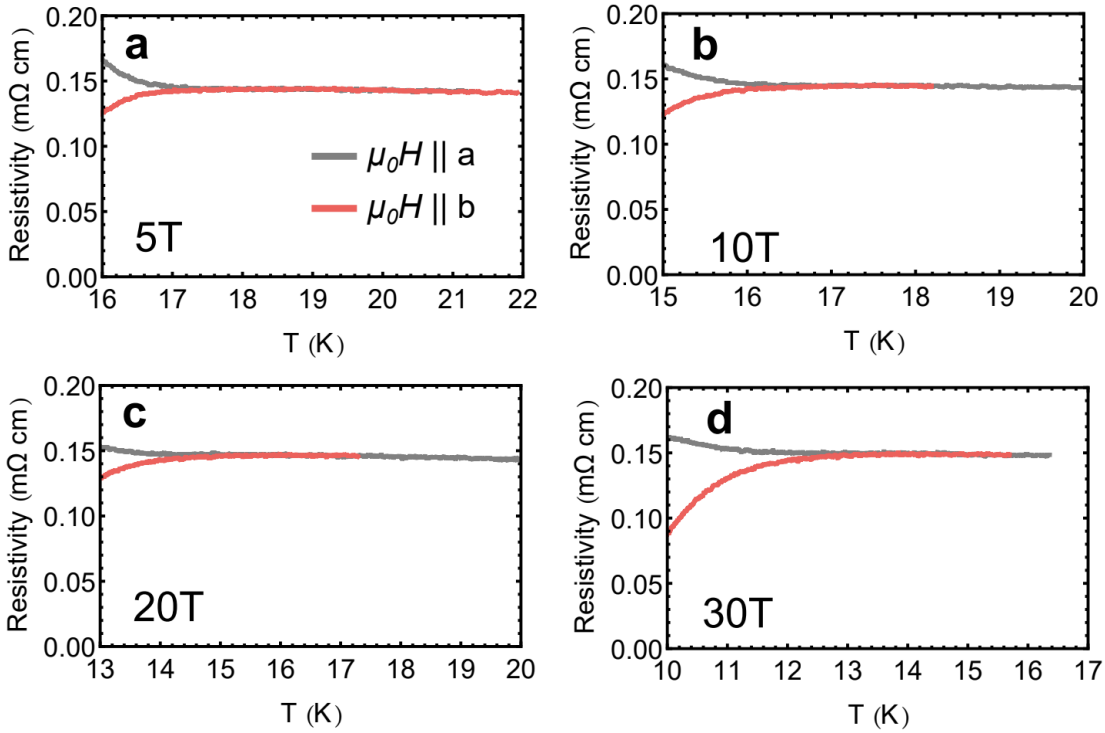

Fig. S6: **Comparison of normal state resistivity anisotropy at high fields in underdoped sample.** (a-d) Field directional dependence of the normal state resistivity at 5, 10, 20, and 30 T. Data in this figure is the same as in Fig. 2(a,c,e) and is presented without scaling. This plot excludes data under $\mu_0 H = 41$ T since there is minimal overlap of the normal state resistivities.

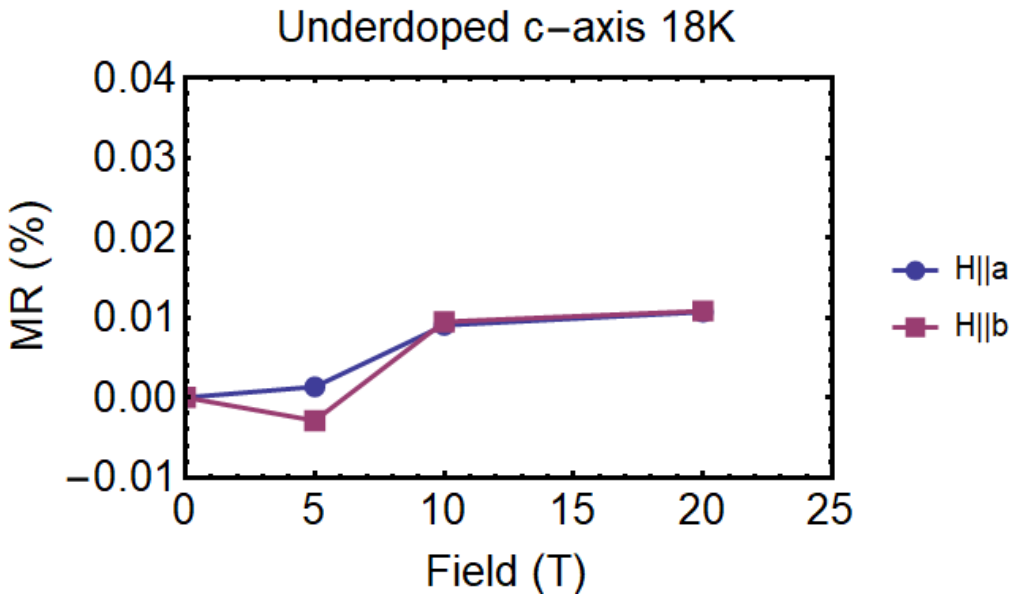

Fig. S7: **Magnetic field dependence of the magnetoresistance at 18 K for underdoped sample.** Magnetoresistance of the underdoped crystal measured with *c*-axis resistivity and fields along the *a* and *b* axes from Fig. 2(a,c,e). The MR is negligible at 1% of 1% and the sample exhibits no in-plane directional field dependence.